Numerical Modeling and Simulation of a Fabry–Perot Sensor for Refractive Index Measurement

Sandisiwe Bangani[1], **James Jena**[2] **and David Waswa**[3]

[1,2,3],Department of Physics, Centre for Broadband Communication, Nelson Mandela University, Port Elizabeth, South Africa

E-mail: s215121457@mandela.ac.za

Abstract. The precise monitoring of chemical concentrations in liquids is critical for environmental, industrial, and biomedical applications. Optical fiber sensors, particularly those based on Fabry-Perot interferometry (FPI), offer high sensitivity, tolerance to harsh environments, and multi-sensing capabilities, making them ideal for detecting refractive index changes in various solutions. This study presents the modeling and simulation of an FPI sensor for real-time monitoring of refractive index changes in sugary aqueous solutions. The reflected spectra were studied using two signal processing techniques: fringe visibility and fast Fourier transform. The obtained sensitivities in refractive index units (RIU)varied between 2.093 nm^{-1}/RIU and 0.582 nm^{-1}/RIU for the latter method and 0.973 dB/RIU when analyzing the fringe visibility. The sensor's size and its all-in-fiber design enable remote and real-time monitoring, making it ideal for use in environmental monitoring, chemical sensing, and biomedical diagnostics.

1 Introduction

The refractive index (RI) is a crucial metric for describing an analyte and is commonly used in biomolecule detection, clinical diagnostics, drug analysis, pollution management, and monitoring [1, 2, 3]. The precise and dependable measurement of the refractive index of gases and liquids enables real-time detection of changes in concentration, contamination, or chemical reactions. While methods like Abbe refractometry [4] and prism-based [5] techniques are precise, traditional RI sensing approaches come with drawbacks: they are expensive, bulky, sensitive to environmental noise, and lack remote sensing capabilities. Optical fiber-based sensors have received significant attention in biological and environmental sensing due to their unique features, including corrosion resistance, immunity to electromagnetic interference, high precision, and compactness [6, 7].

Among different optical fiber sensing setups, fiber-based Fabry-Perot (FP) sensors have attracted considerable attention for refractive index measurements. The working principle of these sensors is based on the interference of multiple reflections in a cavity created by partially reflective surfaces. Modulation of the reflected interference signal occurs due to alterations in the optical path length or reflectivity at the cavity boundaries, resulting from variations in the external refractive index. The surrounding medium's refractive index can be determined through an accurate analysis of such modulation.

Conventional FP interferometric sensors can provide low-cost absolute RI measurements with low thermal sensitivity by modulating the phase of an FP fiber interferometer in response to a change in a physical parameter. FP RI sensors can measure RI with great sensitivity and resolution due to their resonant wavelength response. However, these sensors have some drawbacks, including temperature cross-sensitivity and complicated architectures. Also, according to the Fresnel law, the reflected light from the surface is extremely weak when the RI of the measuring medium is near that of the optical fiber [8]. Therefore, these sensors can only measure materials with a

lower RI than the RI of the core of the fiber, and this limits their practical applications.

In this study, we model and simulate a simple in-line F-P fiber sensor that measures the RI of a sugary solution without requiring the filling of any microscopic fiber cavities. The sensor is created by forming a short air cavity near the tip of a single-mode Germanium-doped fiber through etching and fusion splicing with an unetched fiber. Following splicing, the fiber is cleaved to create the second and third cavities. The reflected light from the fiber tip interferes with the light reflected from the air cavity. The RI of a liquid can be reliably determined by measuring the fringe contrast of its interference pattern in the reflected spectrum. The sensor measures refractive indices greater than air with exceptional linearity and precision, regardless of temperature.

2 Methodology

2.1 Sensor Fabrication

2.1.1 Chemical Etching: A single-mode photosensitive Germanium-doped core fiber is used. The fiber cladding and core are etched with hydrofluoric acid (HF, 50% by weight) for 8 minutes. Acid solutions with appropriate ratios can be used to taper or hollow the fiber tip due to varying etching rates between the core and cladding.
The chemical reaction between HF, germanium, and silica is:

$$SiO_2 + 6HF \rightarrow 2H_3O^3 + SiF_6^{2-}$$

$$GeO_2 + 6HF \rightarrow 2H_3O^3 + GeF_6^{2-}$$

The lower bond dissociation energy of Ge-O bonds (660 KJ/mol) compared to Si-O bonds (799 KJ/mol) [9] allows for faster etching of germanium-doped cores than fused silica cladding.

2.1.2 Fusion Splicing: The next step is to fuse the etched fiber with an unetched fiber. An air gap is generated in the splice, which can be used as a reflector. The size and shape of the air gap, as well as its reflectance and transmittance, are determined by three splicer parameters: fiber overlap, arc power, and arc duration. The last step includes cleaving the tip of the fiber to form the second cavity.

2.2 Sensor Operation Principle

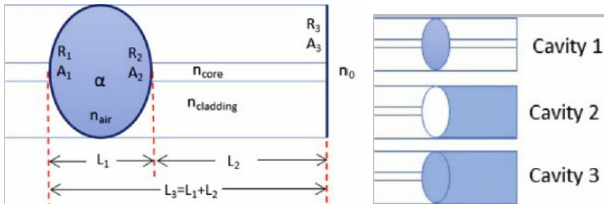

Figure 1: The schematic of the sensor (*left*) sensor head, (*right*) the three cavities Ref. [10].

Figure 1 shows the sensing head that is composed of an air bubble enclosed within the fiber, which functions as an in-line FP interferometer. The first and second reflecting surfaces are the bubble's interfaces, forming the initial resonant cavity. Their reflection coefficients are R_1 and R_2, while their transmission coefficients are A_1 and A_2 (primarily related to surface imperfections). The second cavity is generated between the second and third reflective mirrors, with the latter representing the cleaved end of the fiber. Finally, we consider a third resonant cavity produced between the first and third reflective surfaces, with R_3 and A_3 being the reflecting and transmission coefficients of the third mirror. The cavity loss factor is denoted as α, where n_{core} and $n_{cladding}$ are the refractive indices of the Ge-doped fiber core and silica cladding, respectively, and n0 is the refractive index of the surrounding medium. L_1 and L_2 denote the lengths of cavities 1 and 2. The functioning principle of the sensor is based on the interference of light reflections across the three interfaces. The reflection spectrum's light intensity of the three-beam interferometer can be represented as the sum of the intensities of each surface, plus a phase term, as illustrated below. A more detailed expression is given in [11].

$$R_{reflected} = R_1 + R_2 + R_3 + 2\sqrt{R_1R_2}cos(\phi_1) + 2\sqrt{R_2R_3}cos(\phi_2) + \sqrt{R_1R_3}cos(\phi_3) \quad (1)$$

where,

$$\phi_1 = \frac{4\pi n_{air} L_1}{\lambda}$$

$$\phi_2 = \frac{4\pi n_{Ge} L_2}{\lambda}$$

$$\phi_3 = \frac{4\pi (n_{air} L_1 + n_{Ge} L_2)}{\lambda}$$

The FP interferometer's response to changes in the refractive index of the surrounding medium is determined by the reflected intensity, therefore, fringe visibility is proportional to the reflectance of Mirror 3 (R3) in the fiber's tip.

$$R_3 = (\frac{n_{Ge} - n_{sol}}{n_{Ge} + n_{sol}})^2 \tag{2}$$

where n_{Ge} and n_{sol} are the refractive indices of the Germanium-doped core fiber and those of the sugar solution. When the reflectance in mirror 3 increases, the reflected intensity drops (for $n_{Ge} > n_{sol}$), resulting in the drop in optical power and a decrease in fringe contrast/visibility, given below:

$$V = \frac{I_{max} - I_{min}}{I_{max} + I_{min}} \tag{3}$$

where I_{max} and I_{min} are the maximum and minimum intensities in the reflected spectra.

2.3 Experimental Setup

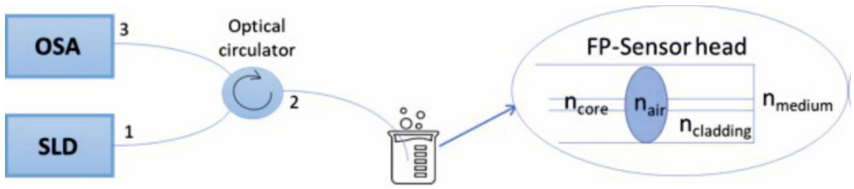

Figure 2: Experimental setup. OSA - Optical Spectrum Analyzer, SLD - superluminescent laser diode. n - refractive index Ref. [10].

The simulation was done in MATLAB. The procedure used for monitoring variations in the refractive index of a sugar solution, shown in Figure 2, a superluminescent laser diode (SLD) is employed, which emits light within a wavelength range of 1500 to 1600 nm. The laser is connected to the FP interferometric sensor dipped in a sugar solution through port 2 of the optical circulator, which also directs the reflected signal from the sensor to the optical spectrum analyzer (OSA) through port 3, where the signal data are obtained. A wavelength range of 1520 to 1555 nm was chosen, and in this region, the signal's fringe contrast or visibility and reflected intensity were used to calculate the solution's refractive index. A fast Fourier transform (FFT) of the reflected spectra was performed, and the amplitudes of the frequency domain signals were correlated with the solution's refractive index.

3 Results and Discussion

Parameter	Value
n_{Ge}	1.47
n_{air}	1.00
L_1	150 μm
L_2	2000 μm
L_3	$L_1 + L_2$

Table 1: Values of parameters used in the calculation of the reflected spectrum for the sensor.

Figure 3 shows the simulated results of the reflected spectra at different sugar concentrations in water, and Table 1 contains the values of the parameters that were used in the calculation of the reflected spectra. An intensity shift can be observed in the signal as a result of an increase in the sugar concentration in the liquid. When sugar

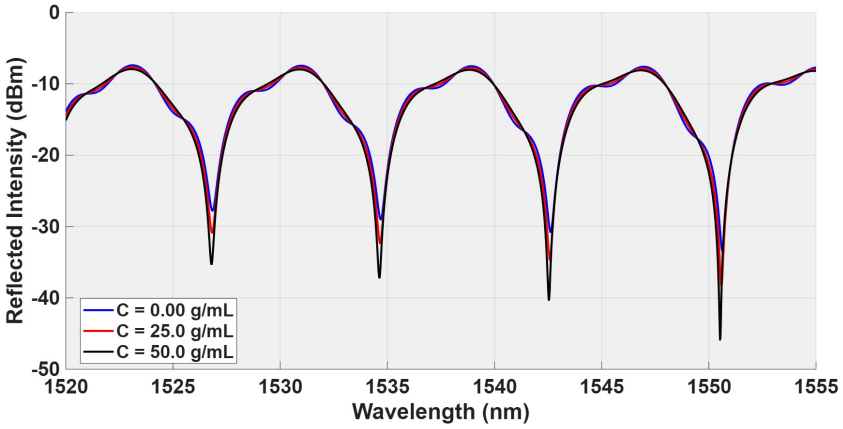

Figure 3: Reflected spectra at different sugar concentration.

concentration increases, the light transmitted from the sensor to the solution interacts with the sugar particles, and some of it is absorbed or scattered; hence, the reflected signal loses intensity.
The visibility or contrast of interference fringes indicates how well bright and dark fringes are separated. Due to changes in the optical path difference (OPD) and the way light waves interfere, the visibility of fringes in interference patterns reduces as a solution's refractive index increases. Higher refractive indices, in particular, reduce the intensity of the reflected signal, which reduces the contrast between bright and dark fringes; this is shown in Figure 4. The achieved change in the fringe contrast (dB) per unit refractive index was 0.973 dB/RIU.

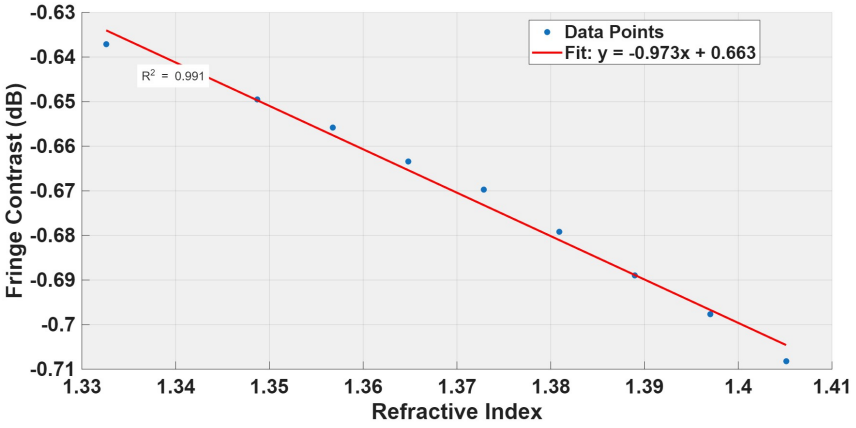

Figure 4: The fringe contrast vs refractive index in the wavelength range of 1520 to 1555 nm.

Figure 5 shows the fast Fourier transform analysis of the reflected spectra. There are three regions of interest in the signals: Peaks 1, 2, and 3. Cavity 1 lies entirely within the fiber or air gap segment, where both the length and refractive index (n_{air}) are constant throughout the experiments. The reflectivity at the two interfaces (mirrors 1 and 2) also remains unchanged, and no part of this cavity is exposed to the solution. As a result, the interference fringe contrast (and thus the FFT amplitude) for this component is constant, independent of the external refractive index.
One of the mirrors in cavity 2 is formed at the fiber-solution interface, that is, mirror 3. Therefore, due to changes in the refractive index of the solution, the reflectivity at this interface also changes, according to equation 2. A lower reflectivity means weaker interference fringes, resulting in a lower FFT amplitude, hence the shape of the graph shown in Figure 6 (*left*). The achieved resolution in cycles per refractive index units in this cavity was 2.093 nm^{-1}/RIU
Cavity 3 includes the full length from mirror 1 to 3, so its reflectivity and interference strength are influenced by both internal and external interfaces. The overall contrast of the fringes reduces as the solution's refractive index

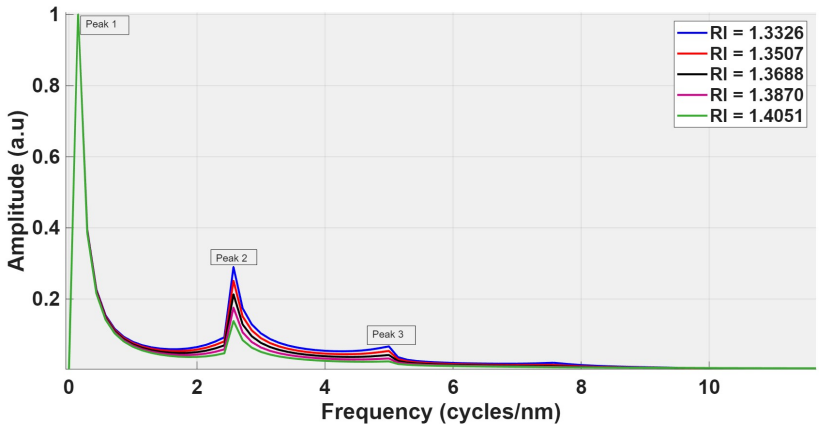

Figure 5: The Fast Fourier Transform of the reflected spectra.

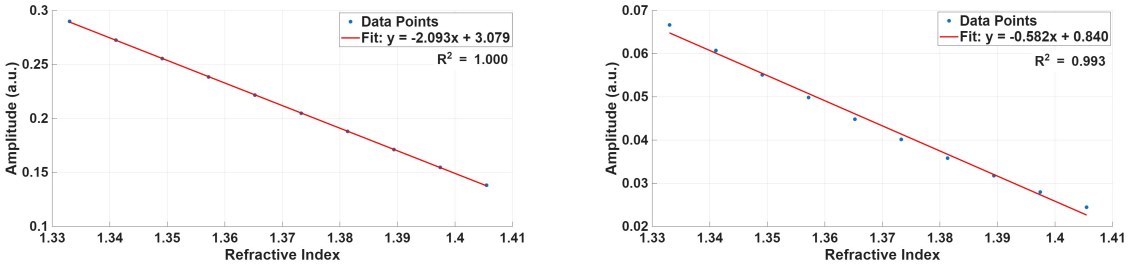

Figure 6: Calibration curves using spectral analysis (*left*) Peak 2, and (*right*) Peak 3 from Figure 5.

increases due to the reduced reflectivity at mirror 3, and increased optical losses at the fiber-solution boundary. Consequently, the amplitude of peak 3 in the FFT also decreases with increasing refractive index at a sensitivity in cycles per refractive index units of 0.582 nm^{-1}/RIU, as shown in Figure 6 (*right*).
Figure 7 shows the changes in refractive index of the solution with increasing sugar concentration, with a sensitivity in refractive index per concentration of 0.0014 RI/C. A solution's refractive index normally increases as its concentration increases because the presence of more solute particles in the solution influences how light passes through it. Specifically, more concentration increases the density of the medium, which causes light to slow down and bend more, resulting in a higher refractive index.

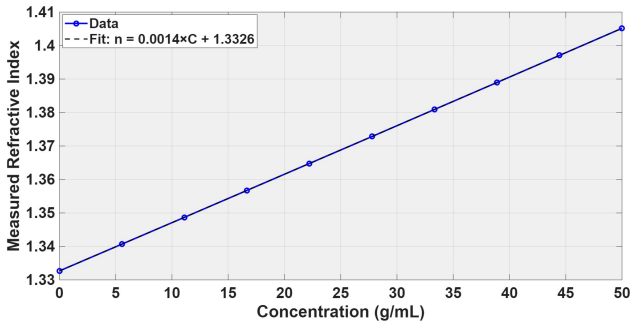

Figure 7: Calibration curve between concentration in the liquid in relation to its corresponding refractive index.

4 Conclusion

In this study, we provide a modeled and simulated approach for constructing in-line fiber Fabry-Perot cavities that involves etching a single-mode Germanium-doped silica core and splicing it to an unetched fiber to create a micrometer-sized air bubble within the fiber. After splicing, the fiber tip was cleaved, generating the sensor's cavities 2 and 3. The performance of the resulting FP interferometric sensor was examined for refractive index sensing of a sugar solution with varying concentration, and a sensitivity of 0.0014 RI/C was achieved through simulation. The reflected spectra were analyzed using two signal processing techniques: fringe contrast/visibility and a fast Fourier transform. The obtained sensitivities ranged between 2.093 nm^{-1}/RIU and approximately 0.582 nm^{-1}/RIU for the latter approach, and around 0.973 dB/RIU for evaluating fringe visibility.
The sensor is highly sensitive to variations in the refractive index, with clear, quantifiable changes in the interference spectrum corresponding to various sugar concentrations in aqueous solutions. The tiny, all-fiber structure allows both remote and real-time operation, making it ideal for chemical sensing, biological diagnostics, and environmental monitoring. The findings confirm that Fabry-Perot interferometric sensors provide a reliable and precise method for measuring refractive index in a variety of liquid media.

Acknowledgements

The author would like to acknowledge the guidance from the supervisors, Dr. David Waswa and Dr. James Jena. The author would also like to acknowledge Telkom's Centre of Excellence and CSIR for the financial support.

References

[1] V. S.-Y. Lin, K. Motesharei, K.-P. S. Dancil, M. J. Sailor, and M. R. Ghadiri, "A porous silicon-based optical interferometric biosensor," *Science*, vol. 278, no. 5339, pp. 840–843, 1997.

[2] F. Vollmer and S. Arnold, "Whispering-gallery-mode biosensing: label-free detection down to single molecules," *Nature methods*, vol. 5, no. 7, pp. 591–596, 2008.

[3] S. G. Patching, "Surface plasmon resonance spectroscopy for characterisation of membrane protein–ligand interactions and its potential for drug discovery," *Biochimica et Biophysica Acta (BBA)-Biomembranes*, vol. 1838, no. 1, pp. 43–55, 2014.

[4] J. Rheims, J. Köser, and T. Wriedt, "Refractive-index measurements in the near-ir using an abbe refractometer," *Measurement Science and Technology*, vol. 8, no. 6, p. 601, 1997.

[5] C.-C. Cheng, "Refractive index measurement by prism autocollimation," *American Journal of Physics*, vol. 82, no. 3, pp. 214–216, 2014.

[6] B. H. Lee, Y. H. Kim, K. S. Park, J. B. Eom, M. J. Kim, B. S. Rho, and H. Y. Choi, "Interferometric fiber optic sensors," *sensors*, vol. 12, no. 3, pp. 2467–2486, 2012.

[7] M. Hirsch, D. Majchrowicz, P. Wierzba, M. Weber, M. Bechelany, and M. Jędrzejewska-Szczerska, "Low-coherence interferometric fiber-optic sensors with potential applications as biosensors," *Sensors*, vol. 17, no. 2, p. 261, 2017.

[8] G. Z. Xiao, A. Adnet, Z. Zhang, F. G. Sun, and C. P. Grover, "Monitoring changes in the refractive index of gases by means of a fiber optic fabry-perot interferometer sensor," *Sensors and Actuators A: Physical*, vol. 118, no. 2, pp. 177–182, 2005.

[9] D. R. Lide, "Crc handbook of chemistry and physics, ; lide, dr, ed," 2006.

[10] M. Nespereira, J. M. Coelho, and J. M. Rebordão, "A refractive index sensor based on a fabry–pérot interferometer manufactured by nir laser microdrilling and electric arc fusion," in *Photonics*, vol. 6, no. 4. MDPI, 2019, p. 109.

[11] Z. L. Ran, Y. J. Rao, W. J. Liu, X. Liao, and K. S. Chiang, "Laser-micromachined fabry-perot optical fiber tip sensor for high-resolution temperature-independent measurement of refractive index," *Optics express*, vol. 16, no. 3, pp. 2252–2263, 2008.